

# High Performance Raster Scanning of Atomic Force Microscopy Using Model-free Repetitive Control

Linlin Li<sup>a,b</sup>, Andrew J. Fleming<sup>c</sup>, Yuen K. Yong<sup>c</sup>, Sumeet S. Aphale<sup>d</sup>, LiMin Zhu<sup>a,e,\*</sup>

<sup>a</sup>State Key Laboratory of Mechanical System and Vibration, School of Mechanical Engineering, Shanghai Jiao Tong University, Shanghai 200240, China

<sup>b</sup>State Key Laboratory of Fluid Power and Mechatronic Systems, Zhejiang University, Hangzhou 310027, China

<sup>c</sup>School of Electrical Engineering and Computing, University of Newcastle, Callaghan NSW 2308, Australia

<sup>d</sup>The Centre for Applied Dynamics Research, School of Engineering, University of Aberdeen, Aberdeen AB24 3UE, UK

<sup>e</sup>The Shanghai Key Laboratory of Networked Manufacturing and Enterprise Information, Shanghai 200240, China

---

## Abstract

The image quality of an atomic force microscope depends on the tracking performance of the lateral X and Y axis positioner. To reduce the requirement for accurate system models, this article describes a method based on Model-free Repetitive Control (MFRC) for high performance control of fast triangular trajectories in the X-axis, and a slow staircase trajectory in the Y-axis, while simultaneously achieving coupling compensation from the X-axis to Y-axis. The design and stability analysis of the MFRC scheme are presented in detail. The tracking results are experimentally evaluated with a range of different load conditions, showing the efficacy of the method with large variations in plant dynamics. To address the coupling from the X-axis to the Y-axis while tracking the non-periodic staircase trajectories, a pre-learning step is used to generate the compensation signals, which is combined in a feedforward manner in real-time implementations. This approach is also applied to address the problem of longer convergence if needed. Experimental tracking control and coupling compensation is demonstrated on a commercially available piezoelectric-actuated scanner. The proposed method reduces the root-mean-square tracking from 191.4 nm in open-loop or 194.6 nm with PI control, to 2.8 nm with PI+MFRC control at 100 Hz scan rate, which demonstrates the significant improvement achieved by the proposed method.

**Keywords:** Atomic Force Microscopy, raster scanning, tracking control, repetitive control, cross-coupling compensation

---

## 1. Introduction

Several discoveries in life science, information, materials, and other disciplines, rely on the extraordinary features of Atomic Force Microscopes (AFMs) for imaging, characterizing, and manipulating matter with a resolution down to the nanoscale [1–3]. In imaging applications, the AFM employs a cantilever with a sharp probe to interrogate

---

\*Corresponding author

Email address: [zhulm@sjtu.edu.cn](mailto:zhulm@sjtu.edu.cn) (LiMin Zhu)

1  
2  
3 over a sample. The surface height of the sample causes the cantilever to deflect, therefore varying the probe-sample  
4 interaction force. This interaction force is regulated using a Z-axis (vertical) controller to keep the deflection of the  
5 cantilever constant. The topography of the sample is measured by the movement or control voltage in the Z-axis.  
6  
7

8 Commonly, raster scanning is selected to generate the AFM images, in which the fast axis (X-axis) is actuated with  
9 a triangular signal and the slow axis (Y-axis) is actuated with the corresponding stair-case or ramp-case signals [4, 5].  
10 To maximize scanning rate for dynamic imaging, there are multiple challenges that degrade the tracking performance  
11 of raster scanning and thus image quality. These include the hysteresis nonlinearity possessed by the piezoelectric  
12 actuators, the lightly-damped resonance of the mechanism, and the cross-coupling effect between the scanning axes  
13 [6]. In particular, under high-frequency inputs, the nonlinearities would be coupled with the vibrations associated  
14 with the lightly-damped resonance, which complicates the control design and limits the speed at which high-precision  
15 AFM images can be obtained [7, 8].  
16  
17  
18  
19

20 During the past decade, significant improvements to the above issues have been made [5, 9–11]. To reduce  
21 the effect of hysteresis, several model-based modeling and compensation methods have been developed, such as  
22 the operator-based models [12, 13] (e.g. Prandtl-Ishlinskii model and Preisach model), intelligent models [14] (e.g.  
23 neural-network model and support vector machine model). It should be noted that the modeling and inversion of the  
24 hysteresis is not trivial, and it may need to be repeated for multiple applications. When hysteresis is coupled with  
25 lightly-damped resonant modes, the compensation performance can degrade dramatically. A variety of control tech-  
26 niques have been developed to address the vibrational problems on the basis of advanced hardware design [15–17],  
27 which include feedforward approaches [18, 19], such as input shaping, optimal trajectory design, and notch-filter-  
28 based techniques, and feedback approaches, such as positive position feedback and its extensions [20, 21], integral  
29 resonant control [22], and delayed position feedback control [23]. Among those techniques, the closed-loop ap-  
30 proaches have better robustness to plant variations in practical implementations, so they are more widely utilized than  
31 feedforward approaches [11, 24, 25]. Further, to realize the tracking application of the nanopositioners, the tracking  
32 controllers are usually incorporated with the above control techniques for mitigating the residual nonlinearities and  
33 other disturbances. For tracking periodic trajectories, the highest performing methods are the learning-based schemes,  
34 repetitive control [26–28] and iterative control [7, 29]. Specifically, it is analyzed in [8] that, the tracking errors in-  
35 duced by the hysteresis nonlinearity exhibit periodic behaviors under periodic inputs, and thus can be mitigated by  
36 these learning-based schemes, making it rather simple for high-precision raster scanning of AFM. It should be noted  
37 that in these developments, the multiple-axis scanners are normally treated as single input and single output systems,  
38 where the cross-coupling is neglected. In fact, the cross-coupling effect would become prominent in large-range and  
39 high-speed scanning operations, especially for these popularly used commercial tube-type scanners, which would  
40 cause tilting and other artifacts in the AFM images [6].  
41  
42  
43  
44  
45  
46  
47  
48  
49  
50  
51  
52  
53

54 The three main research efforts for cross-coupling compensation in the field are (i) model-based cross-coupling  
55 compensation control; (ii) feedback tracking control, and (iii) learning-based schemes. For model-based cross-  
56 coupling compensation control, the main idea is to construct the inverse cross-coupling model using different tech-  
57  
58  
59  
60  
61  
62  
63  
64  
65

1  
2  
3 niques (such as Prandtl-Ishlinskii model [30] and MIMO model predictive control method [31, 32]). The inverse mode  
4 is then used to compensate the cross-coupling effect by the feedforward method. However, the cross-coupling usually  
5 include complex dynamics, which make the modeling procedure very challenging. For feedback tracking control, the  
6 idea of this method is to regard the cross-coupling effects as output disturbances and compensate them by tracking  
7 control techniques, such as  $H_\infty$  control [33] and linear quadratic Gaussian control [34]. For learning-based schemes,  
8 it is experimentally investigated in [6] that, under periodic inputs, the tracking errors induced by the coupling effect  
9 result in periodic behaviors, which allows a new way for cross-coupling compensation. During raster scanning, the  
10 main coupling effect is the influence of the fast axis on the slow axis, which leads to the triangularization of the  
11 staircase trajectory, and possibly large tracking errors. In this sense, the modified repetitive control is successfully  
12 implemented to compensate for the tracking errors that result from the coupling of the fast axis on the slow axis, and  
13 therefore high-precision raster scanning with a scanning rate of 40 Hz is achieved [6]. It should be noted that such  
14 modified repetitive control requires accurate modeling of the inverse system dynamics for best performance. There  
15 are several difficulties associated with plant inversion, including multiple modes [35], non-minimum phase zeros [8],  
16 and model uncertainties due to variations in loads masses, temperature, and humidity while operating the AFMs [36].

17 Focusing the above difficulties, this article describes an improved method of Model-free Repetitive Control (MFR-  
18 C) for applications like AFM which require tracking control of a fast axis and cross-coupling compensation of a slower  
19 axis. In order to avoid modeling the inverse system dynamics, a non-causal FIR low-pass filter is introduced into the  
20 repetitive module which has the advantage of zero phase-lag. This replaces the normally used low-pass zero-phase  
21 filter and the inversion of system dynamics in traditional repetitive control. The stability and convergence analysis  
22 is presented in detail to provide criteria for parameters determination. To achieve better tracking performance with  
23 limited bandwidth of the FIR low-pass filter, smoothed raster scanning [37] is selected in this work, which preserves  
24 the same imaging trajectory but with lower high-frequency components compared to traditional raster scanning. With  
25 the objective of fast convergence for the fast-axis and tracking of the non-periodic staircase trajectory during AFM  
26 raster scanning, a pre-training method is utilized to obtain the effective control signals for both lateral axes, which is  
27 then used as feedforward control. This approach combines a baseline tracking controller for handling non-periodic  
28 disturbances and trajectories. Finally, AFM imaging results are presented to visually demonstrate the advantages of  
29 the proposed method.

30 The distinguished contributions of this paper can be summarized as follows:

31 (1) Tailored for the raster scanning of AFMs, the Model-free Repetitive Control (MFRC) is developed for tracking  
32 periodic trajectories in the X-axis and rejecting the corresponding coupled tracking errors in the Y-axis. This addresses  
33 the universal problem of model uncertainties encountered in practical AFM applications especially due to load change  
34 on the scanner.

35 (2) To handle the excessive iterations before convergence and the aperiodicity of the staircase trajectories in the  
36 Y-axis, a pre-learning step is employed to generate the effective control signals, which works in parallel with the  
37 baseline tracking controller in a feedforward manner.

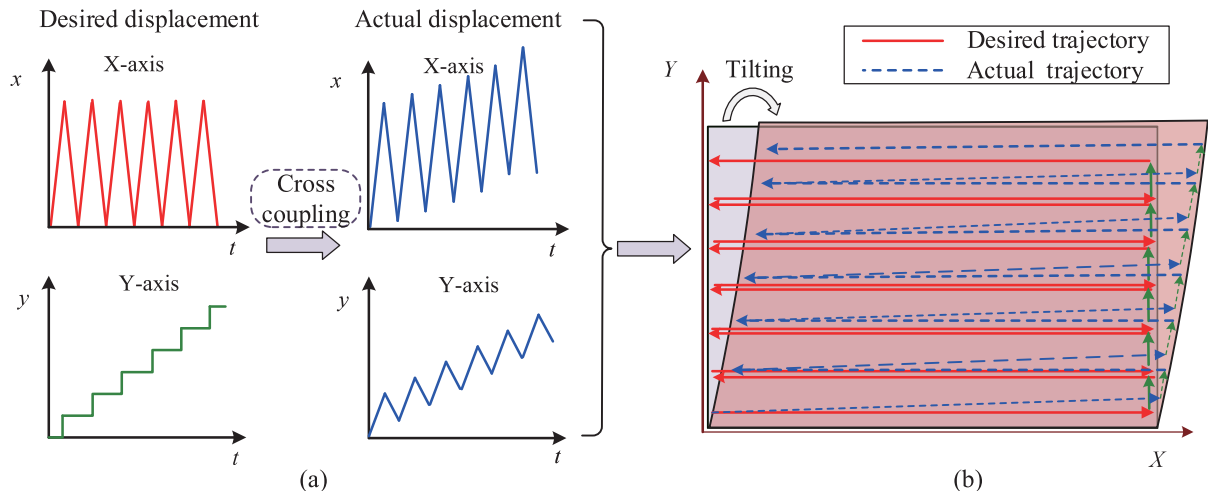


Figure 1: Cross-coupling effect between the lateral X-Y axes in raster scanning of AFM.

(3) Experimental reference tracking and coupling compensation are demonstrated for AFM applications. The images are obtained using a commercially available piezo-actuated scanner, where high-precision raster scanning is demonstrated at 100 Hz, showing the advantages of the proposed schemes.

This paper is outlined as follows. Sec. II provides the basic information of the cross-coupling effect. Sec. III presents the design of the MFRC based scheme, and its stability analysis. Sec. IV presents the details of the experimental setup and the controller performance. The experimental results, including the convergence analysis, tracking results and the AFM imaging results are demonstrated in Sec. V showing the advantages of the proposed scheme for high performance raster scanning. Sec. VI summarizes this paper.

## 2. Cross-coupling information

The cross-coupling effect is significant in many multiple-axis motion control applications. Although several cutting edge mechanical designs can minimize this adverse effect, it cannot be completely avoided due to the errors in machining and assembly [15, 17]. In AFM applications, cross-coupling distorts the scanning trajectories and may introduce artifacts into the captured image [4, 6]. Specially, in raster scanning, the coupling from the fast scanning X-axis on the slow scanning Y-axis causes triangularization of the desired staircase trajectory. Similarly, cross-coupling from the Y-axis on the X-axis causes a drift of the desired triangular trajectory, as illustrated in Fig. 1. Generally speaking, the high-frequency components and the amplitude of the triangular trajectory is much greater than the staircase trajectory [38]. Therefore, this work focuses mainly on the dominant coupling effect of the X-axis on the Y-axis.

It is investigated in [6] that the tracking errors of the Y-axis induced by the coupling effect are found to exhibit periodic characteristics when the X-axis is following a triangular trajectory; therefore, the error can be regarded as a

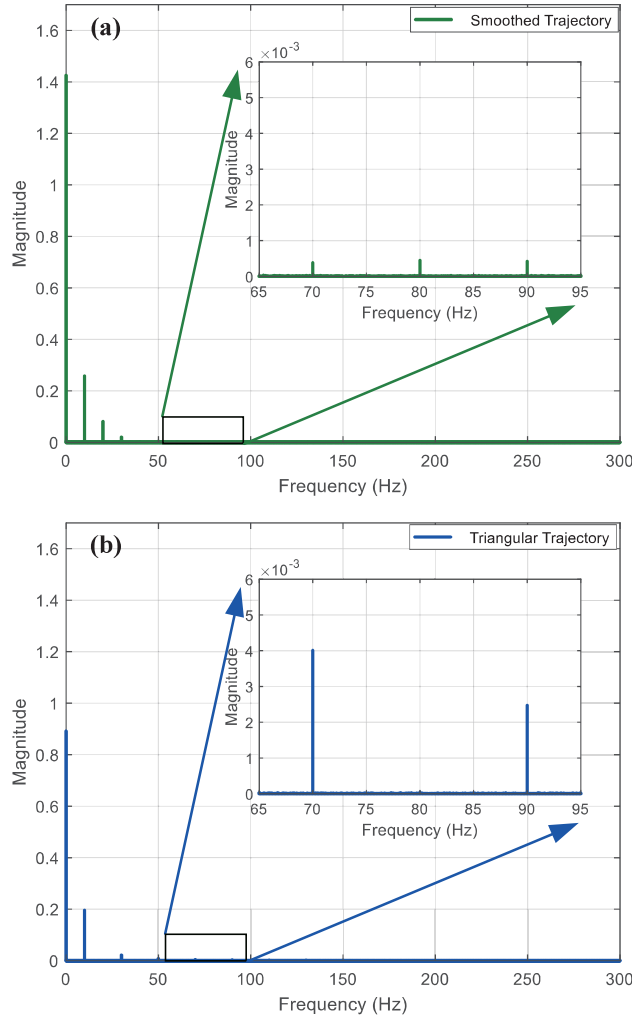


Figure 2: Spectra of the displacement in the Y-axis when the X-axis is tracking different 10-Hz periodic trajectories: (a) Smoothed trajectory; (b) Triangular trajectory.

periodic output disturbance in the Y-axis. To guarantee the stability of the proposed scheme (which will be provided in detail in Sec. III-B), the passband of the designed non-causal FIR low-pass filter is set to a limited range. Since the system bandwidth is limited, high-frequency components of the tracking error are not effectively suppressed. An alternative is to use a smoothed raster scanning method [37] which preserves the original imaging trajectory. The time domain plots of the X-axis and Y-axis (in open-loop) can be found in Fig. 8 and Fig. 9, respectively. Take the scanning rate of 10 Hz for example, the spectrum of the Y-axis position is plotted in Fig. 2(a) and Fig. 2(b), respectively. It can be observed that tracking errors induced by the coupling effect have periodic characteristics. Furthermore, as the high-frequency components of the smoothed trajectory are reduced (investigated in [37]), the high-frequency components of the tracking errors decrease correspondingly. Therefore, the tracking performance is improved using the smoothed raster scanning, which will be comparatively presented in detail in Sec. 5. Based on these observations, the Model-

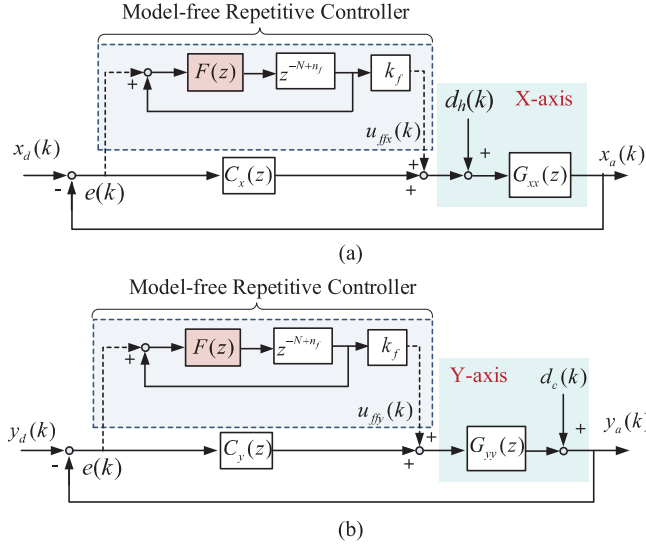


Figure 3: Block diagrams of the MFRC based schemes: (a) X-axis; (b) Y-axis.

free Repetitive Control (MFRC) is developed in this work for control of both lateral axes in high performance raster scanning of AFMs.

### 3. Controller design

In the section, Model-free Repetitive Control is designed for both lateral axes. The stability analysis is provided for parameter selection.

#### 3.1. Design of the Model-free Repetitive Control

For periodic inputs, it is analyzed in [6, 8] that (i) the hysteresis nonlinearity can be regarded as a bounded periodic input disturbances  $d_h(k)$ , and (ii) the coupling effect to the other axis can be seen as a periodic output disturbances  $d_c(k)$  as shown in Fig. 3. In this case, the repetitive control becomes an attractive method for achieving high-precision raster scanning. With the objective of handling the difficulties associated with plant inversion encountered in most repetitive control design, the Model-free Repetitive Control is developed for both lateral axes, which aims for tracking control of the X-axis and coupling compensation for the Y-axis.

Considering the raster scanning, the coupled lateral system can be simplified as Fig. 3, where  $G_{xx}(z)$  and  $G_{yy}(z)$  represents the linear dynamics of the X-axis and Y-axis, respectively. Due to the low variations of the staircase trajectory for Y-axis, the hysteresis nonlinearity of the Y-axis is not considered in Fig. 3. With the minor coupling errors from the Y-axis to the X-axis, this coupling error is not emphasized in this work. The items  $x_d(k)$  and  $x_a(k)$  are the desired trajectory and the actual trajectory for the X-axis, respectively. The items  $y_d(k)$  and  $y_a(k)$  are the desired trajectory and the actual trajectory for the Y-axis. As a plugged-in module, the developed MFRC is designed

in parallel with the baseline tracking controller ( $C_x(z)$  for X-axis and  $C_y(z)$  for Y-axis), whose block diagrams are shown in Fig. 3. In MFRC, a non-causal FIR low-pass filter

$$H(z) = \sum_{i=-n_f}^{n_f} h(i)z^{-i} \quad (1)$$

is introduced into the repetitive loop, instead of the general two-step design of the low-pass filter and inversion of the plant dynamics, where  $n_f$  is the parameter determining the filter length (order). In this way, the complicated modeling process of the inverse dynamics can be avoided, which significantly reduces the problem of model uncertainties and implementation complexity.  $N = f_s/f_d$  is the number of delayed points, where  $f_s$  and  $f_d$  denote the sampling rate and the desired scanning rate, respectively.

The non-causality of  $H(z)$  will be supplemented by the delayed part  $z^{-N}$  in real-time implementation, which becomes

$$F(z) = \sum_{i=0}^{2n_f} h(i)z^{-i} \quad (2)$$

The actual points of the delayed part is therefore reduced to  $N - n_f$ .  $k_f$  is the gain of the developed MFRC. There are many choices for the baseline tracking controller, such as Proportional-Integral (PI) control [39] and sliding mode control [40]. Since the performance of the baseline closed-loop performance is not critical in this work, PI control is selected. It can be concluded from the above that there are only two items ( $F(z)$  and  $k_f$ ) that are required to be determined in MFRC, making it rather simple for practical applications.

### 3.2. Stability analysis

To provide criteria for parameter determination, the condition of stability is analyzed as follows. Since the control schemes for the X-axis and Y-axis are identical, the stability analysis for the X-axis (Fig. 3(a)) is presented as example. Before the design of the developed MFRC, the system with the baseline tracking controller should be designed to ensure asymptotical stability, which implies that  $1 + C_x(z)G_{xx}(z) = 0$  has no roots outside of the unit circle in the  $z$ -plane. Assuming this condition is satisfied first, the sensitivity function is

$$\frac{e(k)}{x_d(k)} = \frac{1 - F(z)z^{-N+n_f}}{[1 + C_x(z)G_{xx}(z)][1 - F(z)z^{-N+n_f}] + F(z)z^{-N+n_f}k_fG_{xx}(z)} \quad (3)$$

Thus, the polynomial of the closed-loop characteristics is (the symbol of  $z$ -domain is ignored in the follow derivation for simplicity)

$$\begin{aligned} D(z) &= (1 + C_xG_{xx})(1 - Fz^{-N+n_f}) + (Fz^{-N+n_f}k_fG_{xx}) \\ &= (1 + C_xG_{xx})(1 - Fz^{-N+n_f} + \frac{Fz^{-N+n_f}k_fG_{xx}}{1+C_xG_{xx}}) \end{aligned} \quad (4)$$

As the first item is asymptotically stable by the previous assumption, the stability depends on the second item only.

According to the Small-gain Theorem, the system is asymptotically stable if

$$\left| -Fz^{-N+n_f} + \frac{Fz^{-N+n_f}k_fG_{xx}}{1 + C_xG_{xx}} \right|_{z=e^{j\omega T_s}} < 1, \omega \in [0, \pi/T_s] \quad (5)$$

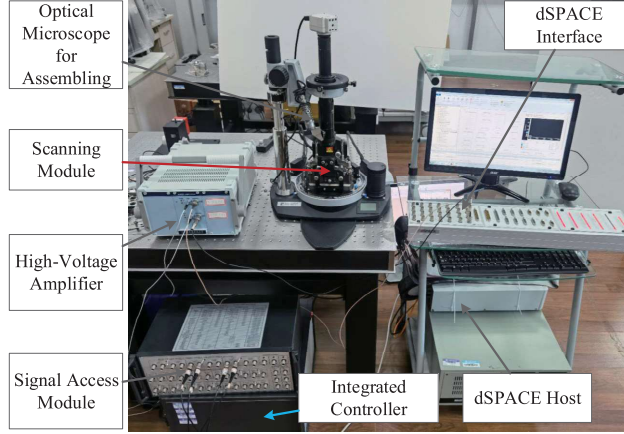


Figure 4: Experimental setup verifying the advantages the developed MFRC scheme.

It is obvious that  $\left|z^{-N+n_f}\right|_{z=e^{j\omega T_s}} = 1$ , then we have

$$\left| -F + \frac{Fk_f G_{xx}}{1 + C_x G_{xx}} \right|_{z=e^{j\omega T_s}} < 1, \omega \in [0, \pi/T_s] \quad (6)$$

which can be expressed as

$$0 < \left| \frac{k_f G_{xx}}{1 + C_x G_{xx}} \right|_{z=e^{j\omega T_s}} < \left| \frac{2}{F} \right|_{z=e^{j\omega T_s}}, \omega \in [0, \pi/T_s] \quad (7)$$

Therefore, the closed-loop system is stable when the control gain satisfies the following condition.

$$0 < k_f < \left| \frac{2+2C_x G_{xx}}{F G_{xx}} \right|_{z=e^{j\omega T_s}} = \left| \frac{2}{F G_{xx}} + \frac{2C_x}{F} \right|_{z=e^{j\omega T_s}}, \quad \omega \in [0, \pi/T_s] \quad (8)$$

It can be observed from Eq. (8) that the FIR low-pass filter should be able to effectively suppress the lightly-damped resonant peak of the scanner to guarantee the availability of the stable control gain.

## 4. Experimental setup and controller implementation

### 4.1. Experimental setup

To demonstrate the effectiveness of the developed MFRC on AFM raster scanning, the experiments are conducted on a commercial AFM (NTMDT, Prima), which includes a piezoelectric tube scanner (PTS) for XYZ positioning. The experimental setup is shown in Fig. 4, which includes the PTS scanning module, the high-voltage amplifier (amplification ratio of 30) providing the actuation voltage for both lateral axes, the signal access module transferring the control signals to the PTS, and the integrated controller outputting the real time sensors signals, the rapid prototype control module (dSPACE, ds1103) running different control schemes and an auxiliary optical microscope adjusting the lasers and sample positions. Each axis of the PTS is equipped with a capacitive displacement sensor. The control



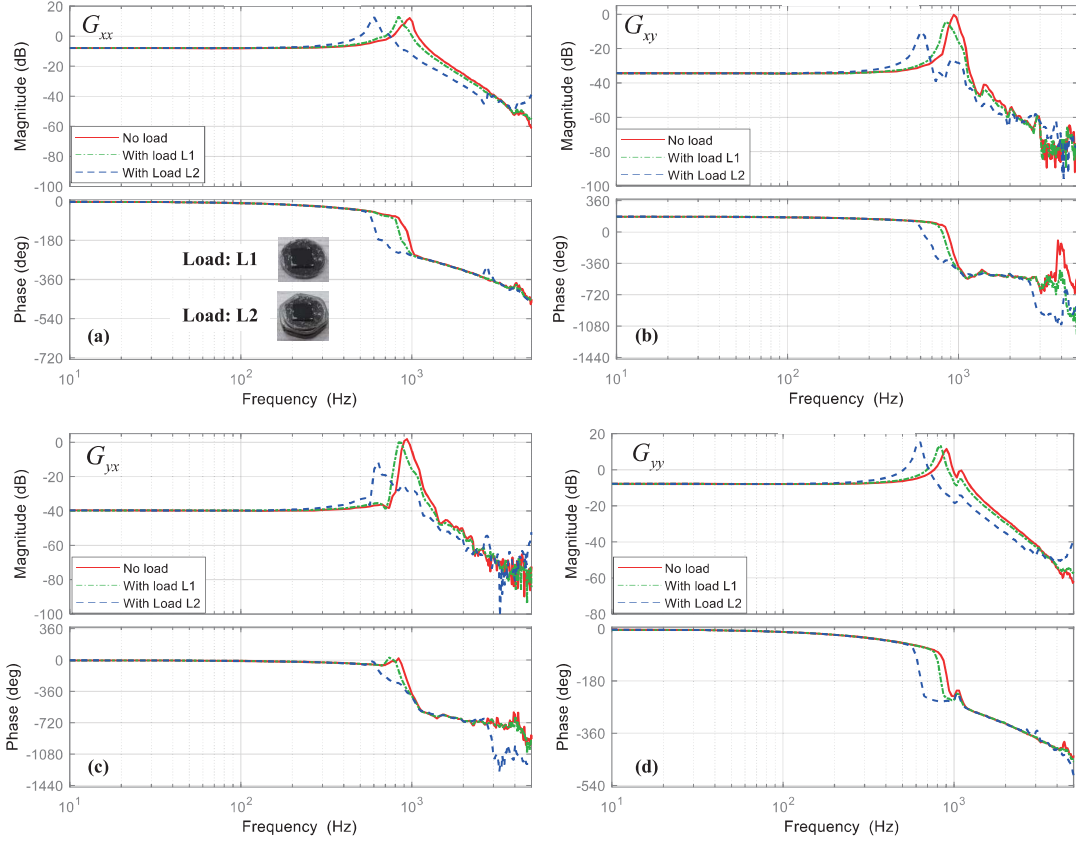


Figure 5: Dynamics of the lateral axes of PTS with different loads: (a) X-axis; (b) The coupling effect from X-axis to Y-axis; (c) The coupling effect from Y-axis to X-axis; (d) Y-axis.

schemes are designed with the environments of Matlab, downloaded to dSPACE host, and operated via the ControlDesk software. For generating the AFM images, a calibration grating (NTMDT, TGQ1) with a rectangular profile (height of  $20nm$ , period of  $3\mu m$ ) is placed on the scanner. The contact probe (Scansens, HA\_C/15) with a resonance of  $19\text{ kHz}$  and a force constant of  $0.26\text{ N/m}$  is employed to measure the sample topography. The sampling frequency is  $20\text{ kHz}$  and thus the imaging resolution is  $100 \times 100$ .

#### 4.2. Controller implementation and performance evaluation

To show the complex dynamics of the scanner and the complicated cross-coupling effect, the dynamics of the lateral axes are investigated first. The low-amplitude bandlimited noise signals are applied to excite the two axes respectively, and the actuation signals and the sensors signal are captured simultaneously. Via identification toolbox of Matlab, the obtained frequency responses are shown in Fig. 5. It can be observed from this figure that the cross-coupling effect shows complex dynamics, making it challenging for cross-coupling modeling. Meanwhile, the multi-modes can be found in the dynamics of the Y-axis. Another problem that usually exists in AFM applications is model uncertainties due to the load (including the sample and holders). To show this, the frequency responses with different

1  
2  
3 samples (no load, with load L1 and with load L2) are analyzed and plotted in Fig. 5 as well. Taking the X-axis for  
4 example, its first-order resonant frequency varies from to 970 to 602 Hz, which is a quite large model uncertainty. This  
5 might lead to the instability of control schemes. However, from Eq. (8), when the closed-loop system is asymptotically  
6 stable for the extreme condition (Load L2 in this work), it would be asymptotically stable for all cases. Without loss  
7 of generality, the two cases (with load L1 and L2) will be considered in the following studies.

8  
9  
10 Before the design of the developed MFRC, the baseline tracking controllers for the X- and Y-axis have to be  
11 optimized. To achieve sufficient tracking performance, the proportional and integral gains of the PI controller is  
12 maximized until the vibrations occur during step response using trial-and-error method, and the resulting parameters  
13 are 0.01 and 300 for the X-axis, and 0.01 and 250 for the Y-axis, respectively. These controller gains are used for all  
14 of the following experiments.

15  
16  
17 Secondly, as the lowest resonant frequencies of the X-axis and Y-axis are about 602 Hz and 635 Hz, the stopband  
18 of  $F(z)$  is set to 600 Hz. Fig. 2 shows that tracking errors are mainly composed of the first three harmonics; therefore,  
19 the passband of  $F(z)$  is set to 300 Hz. To guarantee the behavior of  $F(z)$  within the passband, the Equiripple method  
20 [41] is employed to calculate the filter parameters. With the tradeoff of precision and causality of the developed  
21 MFRC, the order of  $F(z)$  is chosen as 300. Based on the above parameters, the control gain  $k_f$  is optimized as 0.5 via  
22 experiments within the region of stability.

23  
24  
25 To further investigate the performance of the developed MFRC for tracking periodic trajectories and rejecting  
26 periodic disturbances, the magnitude responses of the repetitive loop  $F(z)z^{-N+n_f}/(1 - F(z)z^{-N+n_f})$  and the sensitivity  
27 functions (Eq. (3) ) are presented for the X-axis (with Load L1 and Load L2) in Fig. 6(a) and (b) respectively for  
28 a scanning rate of 100 Hz. It can be observed in Fig. 6(a) that the MFRC mainly generates control gain within the  
29 passband of 300 Hz, and thus rejects the tracking errors distributed within the passband. This can also be concluded  
30 from the sensitivity functions in Fig. 6(b). Additionally, it can also be seen in Fig. 6(b) that the sensitivity functions  
31 for the X-axis with different loads show similar disturbance rejection, demonstrating the robustness of the developed  
32 PI+MFRC against model uncertainties.

## 33 34 35 **5. Experimental studies**

### 36 37 38 *5.1. Tracking results of the X-axis*

39  
40  
41 In raster scanning applications, the control objective for the X-axis is to track a pre-defined triangular trajectory,  
42 which is studied first in this section. The tracking experiments for the smoothed triangular trajectories and the tri-  
43 angular trajectories, with the scanning range of  $10\mu m \times 10\mu m$  and frequencies of 10, 50 and 100 Hz, are conducted  
44 using the developed PI+MFRC on the setup presented in Sec. III. The tracking results of the scanner with the two  
45 different loads are presented in Fig. 7 for the scanning rate of 100 Hz as case studies. It can be observed in Fig. 7,  
46 that the tracking error with a triangular trajectory is larger than a smoothed triangular trajectory. Therefore, smoothed  
47 raster scanning is employed in this work for high-precision scanning applications. From the convergence and the

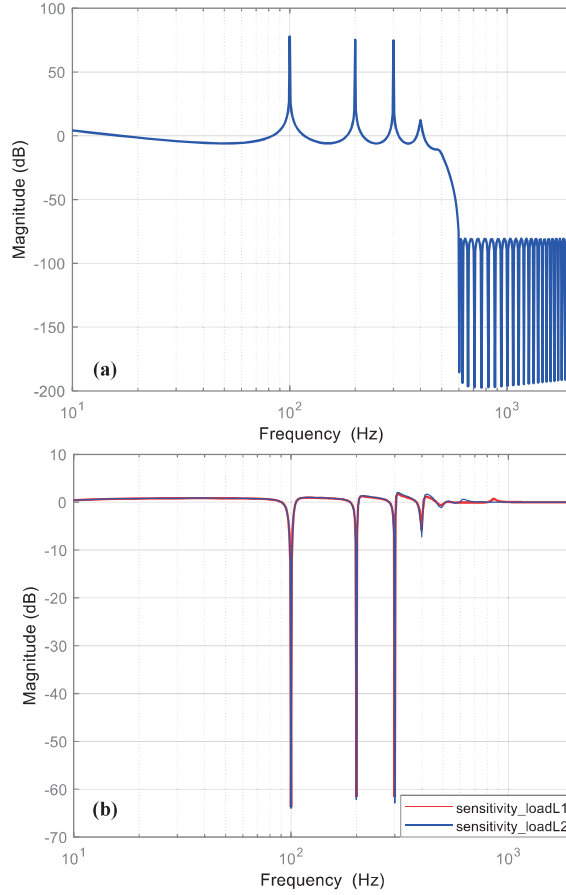


Figure 6: Magnitude response of (a)  $F(z)z^{-N+n_f}/(1 - F(z)z^{-N+n_f})$  and (b) sensitivity functions, for a scanning rate of 100 Hz.

tracking errors in steady-state (Fig. 7 (b) and (c)) for these two trajectories, the tracking results of the scanner with different loads (L1 and L2) resemble each other, which verifies the robustness of developed PI+MFRC against model uncertainties. Hence, the tracking results of the scanner with only load L1 are provided in subsequent section for illustration.

Compared to other model-based repetitive control methods, the developed PI+MFRC scheme requires more iterations to converge to steady-state. To address this issue, the corresponding control signals  $u_{ffx}(k)$  (in Fig. 3) are captured and recorded. These control signals are then regarded as the offline-learned MFRC based feedforward control (MFRCFF), which is combined with the baseline PI controller forming the proposed PI+MFRCFF scheme. In this case, the MFRC in Fig. 3(a) is substituted by  $u_{ffx}(k)$ . The tracking results of the smoothed triangular trajectories with frequencies of 10, 50, and 100 Hz are shown in Fig. 8, where high performance tracking control is achieved in terms of the tracking precision and convergence speed. To show its advantages, the comparative experiments are conducted with different control schemes, which are the baseline PI control and open-loop control. The tracking results in the X-axis for different trajectories and frequencies are also plotted in Fig. 8. In Fig. 8, the hysteresis nonlinearity and

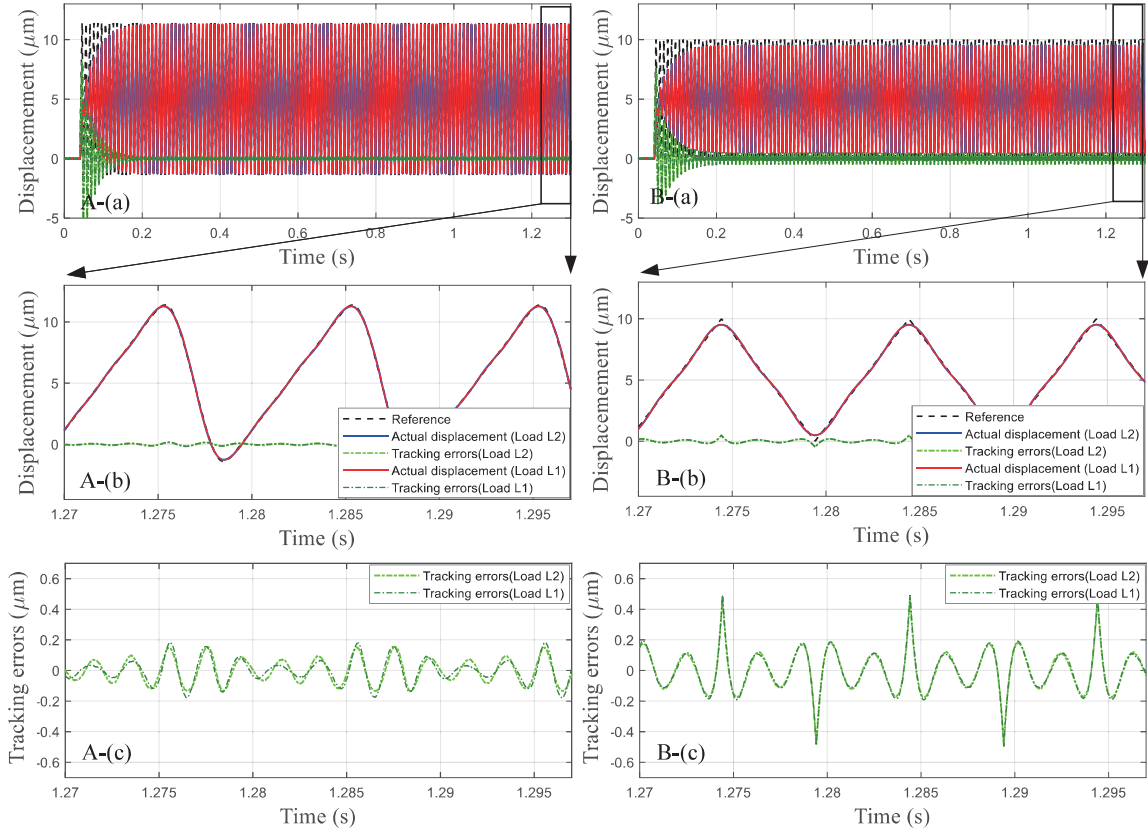


Figure 7: Tracking results of the closed-loop system with different loads under the developed PI+MFRC for different tracking trajectories with the scanning rate of 100 Hz: (A) smoothed trajectory; (B) triangular trajectory.

vibration cause large tracking errors in open-loop, which are both mitigated by the proposed PI+MFRCFF scheme. The tracking performance of the baseline PI controller is also significantly improved greatly by adding the MFRCFF scheme. These results verify the advantages of the proposed PI+MFRCFF scheme in raster scanning applications.

### 5.2. Tracking results of the Y-axis

To investigate the coupling effect from the X-axis to the Y-axis, the tracking results of Y-axis for a constant setpoint (zero) and different control schemes are presented in Fig. 9. In these results, the X-axis is following a smoothed triangular trajectory using the proposed PI+MFRCFF scheme with a scan rate of 10, 50 and 100 Hz. As shown in Fig. 5(b), the coupling dynamics from the X-axis to Y-axis is approximately constants within the frequencies below 300 Hz, so the coupled tracking errors of the Y-axis in open-loop show similar profiles for all tested frequencies. When the Y-axis is under PI control, the coupled tracking errors increase with frequency due to the narrow control bandwidth. For frequencies of 50 Hz and 100 Hz, the error under PI control is similar those in open-loop, which will cause failure of coupling compensation. In contrast, the tracking results of the Y-axis with the developed PI+MFRC show excellent coupling error rejection.

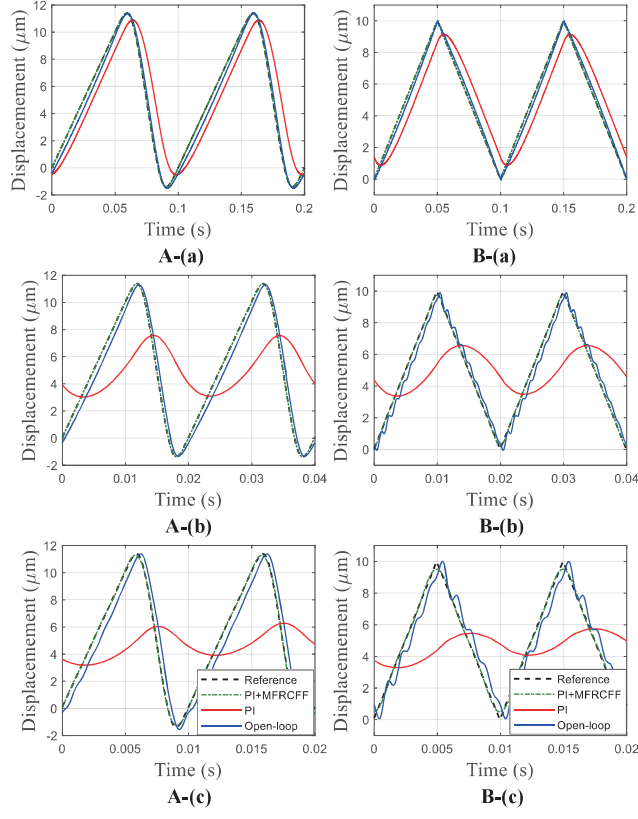


Figure 8: Tracking results for the X-axis with different control schemes under different frequencies: (A) smoothed triangular trajectories; (B) triangular trajectories; (a) 10 Hz; (b) 50 Hz; (c) 100 Hz.

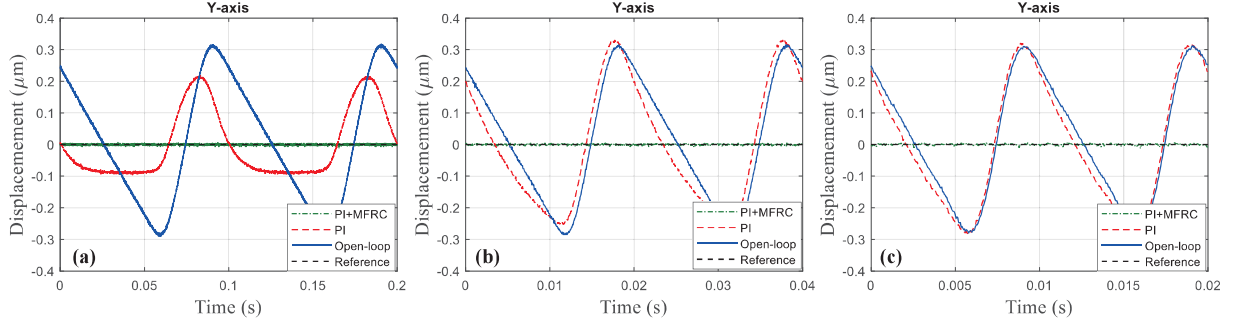


Figure 9: The tracking results of the closed-loop system for Y-axis with different control schemes under different tracking frequencies: (a) 10 Hz; (b) 50 Hz; (c) 100 Hz.

To evaluate the coupling compensation performance, two metrics are calculated, which are the maximum tracking error

$$e_m = \max_{t \in (0, 2T]} |y_d(t) - y_a(t)| \quad (9)$$

Table 1: The coupling induced tracking errors in the Y-axis with different control schemes when X-axis is tracking smoothed triangular trajectories under the proposed PI+MFRCCFF scheme under different frequencies.

Frequency (Hz)	Open-loop (nm)		Baseline PI (nm)		PI+MFRC (nm)	
	$e_m$	$e_{rms}$	$e_m$	$e_{rms}$	$e_m$	$e_{rms}$
10	317.9	191.4	218.7	107.1	7.6	2.5
50	315.3	191.0	330.6	188.5	7.6	2.6
100	312.8	191.4	320.4	194.6	7.6	2.8

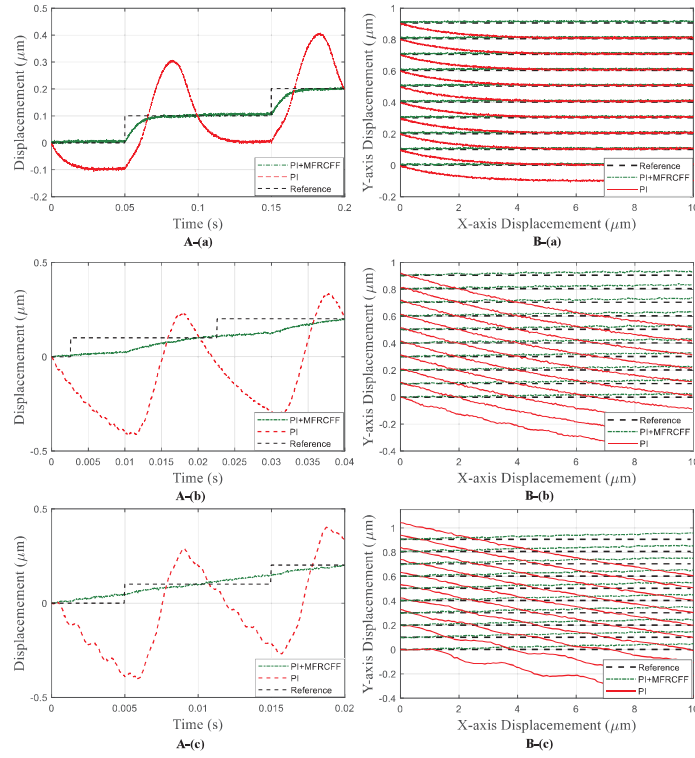


Figure 10: Tracking results of the closed-loop system (with X-axis under PI+MFRCCFF and Y-axis under different control schemes) for different tracking frequencies: (a) 10 Hz; (b) 50 Hz; (c) 100 Hz; (A) tracking results of Y-axis; (B) tracking results in X-Y plane.

and the root-mean-square (RMS) tracking error

$$e_{rms} = \sqrt{\frac{1}{2T} \int_0^{2T} [y_d(t) - y_a(t)]^2 dt} \quad (10)$$

The results are summarized in Table 1. Specifically, it can be seen that the coupled RMS tracking errors under PI+MFRC are reduced from 191.4 nm (in open-loop) and 194.6 nm (with PI) to 2.8 nm at the frequency of 100 Hz, which are reduced by 98.54% and 98.56% respectively, showing the advantage of the developed PI+MFRC scheme for coupling compensation.

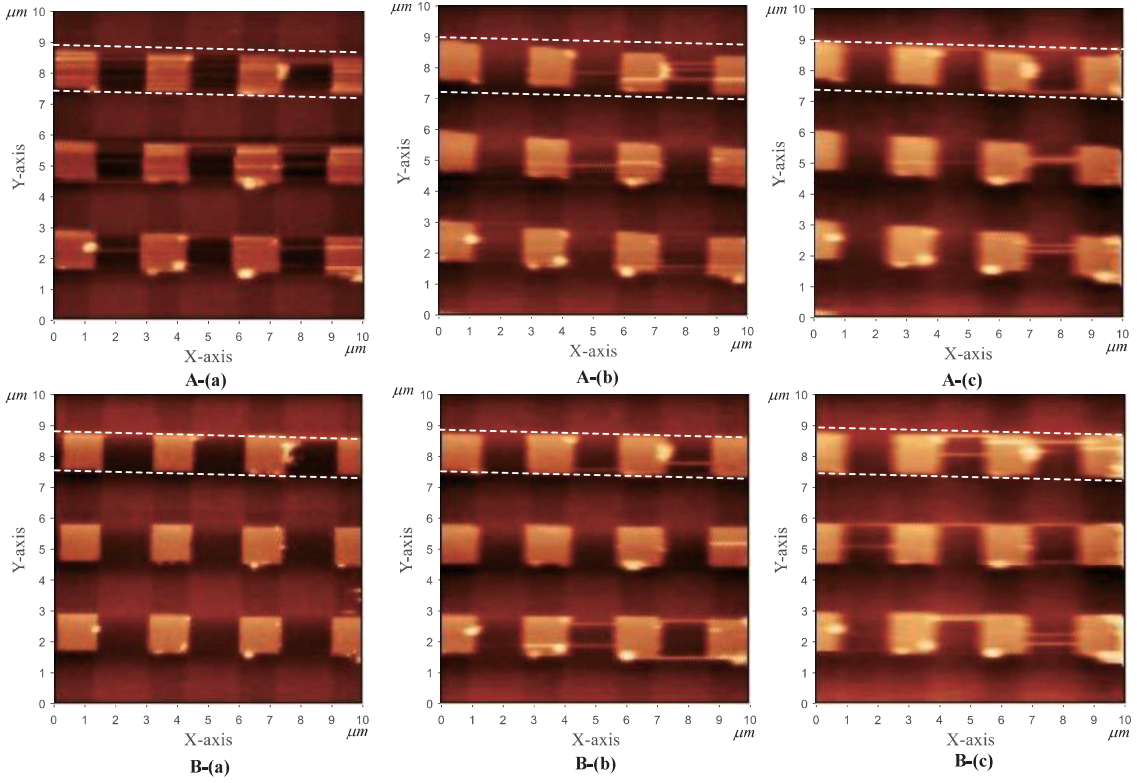


Figure 11: AFM imaging results using smoothed raster scanning for different scanning rates and Y-axis with (A) PI and (B) PI+ MFRCCFF; for the frequency of (a) 10 Hz; (b) 50 Hz; (c) 100 Hz.

### 5.3. Raster scanning and imaging results

In scanning applications, the Y-axis follows nonperiodic staircase trajectory, which hinders the application the developed PI+MFRC scheme. To deal with this problem, the proposed MFRCFF in Sec. V-A is employed herewith, in which the MFRC learned control signals  $u_{ffy}(k)$  are used as the feedforward controller. In this case, the MFRC in Fig. 3(b) is substituted by the  $u_{ffy}(k)$ . To study the effectiveness of the proposed PI+MFRCFF, the smoothed raster scanning experiments are conducted. The tracking results of the X-axis for smoothed triangular trajectories are shown in Fig. 8, while the tracking results of the Y-axis for staircase trajectories and the corresponding raster scanning results (10 lines) are presented in Fig. 10. It can be observed in detail that the scanning trajectories tilt from the desired positions with PI control due to the coupling effect. Since the coupled errors are well compensated using the proposed PI+MFRCFF scheme, raster scanning with this approach generates excellent tracking. Note that due to the narrow bandwidth of the baseline PI control, the tracking performance of the staircase trajectories (under the proposed PI+MFRCFF control) degrades with increasing scan rate, which can be improved by other high-bandwidth tracking methods.

To illustrate the effectiveness of the proposed PI+MFRCFF scheme on AFM imaging applications (especially on coupling compensation), the calibration grating is imaged in Figure 11. The AFM is operated in constant height

1  
2  
3 mode, which implies that the deflection signals of the cantilever are used for generating the AFM images. In Figure  
4 11, the results obtained with PI control are illustrated in the first row and the results obtained with the proposed PI+  
5 MFRCFF scheme are illustrated in the second row. Since all images use the proposed PI+ MFRCFF scheme, the  
6 imaging results show the same features along the X-axis. However, it can be observed in Fig. 11 that the captured  
7 topography under PI control is severely rotated due to the coupling errors. This problem is well addressed using the  
8 proposed PI+ MFRCFF scheme.  
9  
10  
11  
12  
13

## 14 6. Conclusion

15  
16 In this article, a method based on model-free repetitive control is proposed for high performance raster scanning  
17 in AFM applications. The objective is to achieve fast reference tracking in the X-axis, while compensating for the  
18 coupling effect in the Y-axis. The proposed method avoids the need for an inverse system model. Stability analysis  
19 is presented to provide criteria for determining controller parameters. The efficacy of the developed MFRC scheme  
20 is successfully evaluated by controlling an AFM scanner under varying load conditions. To achieve fast convergence  
21 in the X-axis and coupling compensation for staircase trajectories in the Y-axis, a pre-learning step is utilized to  
22 generate the corresponding control signals, which is combined with the baseline PI controller in a feedforward manner.  
23 Experimental results on a piezoelectric tube scanner show significant reductions in X-axis tracking error and Y-axis  
24 coupling error.  
25  
26  
27  
28  
29  
30  
31

## 32 Acknowledgments

33  
34 This work was partially supported by the National Natural Science Foundation of China under Grant Nos. 52105581,  
35 U2013211, and 51975375, the China Postdoctoral Science Foundation (No. 2021M692065), and the Open Founda-  
36 tion of the State Key Laboratory of Fluid Power and Mechatronic Systems, China under Grant No. GZKF-202003,  
37 and the CDSC Scholarship, University of Newcastle, Australia, awarded to Linlin Li.  
38  
39  
40  
41  
42

## 43 References

- 44  
45 [1] G. Binnig and C. F. Quate, "Atomic force microscope," *Phys. Rev. Lett.*, no. 56, pp. 930-933, 1986.  
46 [2] M. Krieg, G. Flaschner, D. Alsteens, et al., "Atomic force microscopy-based mechanobiology," *Nat. Rev. Phys.*, vol. 1, no. 1, pp. 41-57, Jan.  
47 2019.  
48 [3] X. Chen, J. Lai, Y. Shen, Q. Chen, and L. Chen, "Functional Scanning Force Microscopy for Energy Nanodevices," *Adv. Mater.*, vol. 30, no.  
49 48, p. 1802490, Nov. 2018.  
50 [4] M. S. Rana, H. R. Pota, and I. R. Petersen, "Improvement in the Imaging Performance of Atomic Force Microscopy: A Survey," *IEEE Trans.*  
51 *Autom. Sci. Eng.*, vol. 14, no. 2, pp. 1265-1285, Apr. 2017.  
52 [5] S. K. Das, F. R. Badal, Md. A. Rahman, et al., "Improvement of Alternative Non-Raster Scanning Methods for High Speed Atomic Force  
53 Microscopy: A Review," *IEEE Access*, vol. 7, pp. 115603-115624, 2019.  
54 [6] L. Li, C.-X. Li, G. Gu, and L. Zhu, "Modified Repetitive Control Based Cross-Coupling Compensation Approach for the Piezoelectric Tube  
55 Scanner of Atomic Force Microscopes," *IEEE/ASME Trans. Mechatron.*, vol. 24, no. 2, pp. 666-676, Apr. 2019.  
56  
57  
58  
59  
60  
61  
62  
63  
64  
65



- 1  
2  
3  
4 [7] Y. Wu and Q. Zou, "Iterative Control Approach to Compensate for Both the Hysteresis and the Dynamics Effects of Piezo Actuators," *IEEE Trans. Control Syst. Technol.*, vol. 15, no. 5, pp. 936-944, Sep. 2007.
- 5  
6 [8] C.-X. Li and L.-M. Zhu, "High-Speed Tracking of a Nanopositioning Stage Using Modified Repetitive Control," *IEEE Trans. Autom. Sci. Eng.*, vol. 14, no. 3, pp. 1467-1477, 2017.
- 7  
8 [9] Q. Xu, "Adaptive Integral Terminal Third-Order Finite-Time Sliding-Mode Strategy for Robust Nanopositioning Control," *IEEE Trans. Ind. Electron.*, vol. 68, no. 7, pp. 6161-6170, Jul. 2021.
- 9  
10 [10] L. Kong, D. Li, J. Zou, and W. He, "Neural Networks Based Learning Control for a Piezoelectric Nanopositioning System," *IEEE/ASME Trans. Mechatron.*, vol. 25, no. 6, pp. 2904-2914, Dec. 2020.
- 11  
12 [11] G.-Y. Gu, L.-M. Zhu, C.-Y. Su, and H. Ding, "Modeling and Control of Piezo-Actuated Nanopositioning Stages: A Survey," *IEEE Trans. Autom. Sci. Eng.*, vol. 13, no. 1, pp. 313-332, 2016.
- 13  
14 [12] V. Hassani, T. Tjahjowidodo, and T. N. Do, "A survey on hysteresis modeling, identification and control," *Mech. Syst. Signal Process.*, vol. 49, no. 1-2, pp. 209-233, Dec. 2014.
- 15  
16 [13] D. V. Sabarianand, P. Karthikeyan, and T. Muthuramalingam, "A review on control strategies for compensation of hysteresis and creep on piezoelectric actuators based micro systems," *Mech. Syst. Signal Process.*, vol. 140, p. 106634, Jun. 2020.
- 17  
18 [14] P.-K. Wong, Q. Xu, C.-M. Vong, and H.-C. Wong, "Rate-Dependent Hysteresis Modeling and Control of a Piezostage Using Online Support Vector Machine and Relevance Vector Machine," *IEEE Trans. Ind. Electron.*, vol. 59, no. 4, pp. 1988-2001, Apr. 2012.
- 19  
20 [15] K. Cai, X. He, Y. Tian, et al., "Design of a XYZ scanner for home-made high-speed atomic force microscopy," *Microsyst. Technol.*, vol. 24, no. 7, pp. 3123-3132, Jul. 2018.
- 21  
22 [16] D. S. Raghunvanshi, S. I. Moore, A. J. Fleming, and Y. K. Yong, "Electrode Configurations for Piezoelectric Tube Actuators With Improved Scan Range and Reduced Cross-Coupling," *IEEE/ASME Trans. Mechatron.*, vol. 25, no. 3, pp. 1479-1486, Jun. 2020.
- 23  
24 [17] C.-X. Li, G.-Y. Gu, M.-J. Yang, and L.-M. Zhu, "Design, analysis and testing of a parallel-kinematic high-bandwidth XY nanopositioning stage," *Rev. Sci. Instrum.*, vol. 84, no. 12, p. 125111, Dec. 2013.
- 25  
26 [18] A. J. Fleming and A. G. Wills, "Optimal Periodic Trajectories for Band-Limited Systems," *IEEE Trans. Control Syst. Technol.*, vol. 17, no. 3, pp. 552-562, May 2009.
- 27  
28 [19] K. K. Leang and S. Devasia, "Feedback-Linearized Inverse Feedforward for Creep, Hysteresis, and Vibration Compensation in AFM Piezoactuators," *IEEE Trans. Control Syst. Technol.*, vol. 15, no. 5, pp. 927-935, 2007.
- 29  
30 [20] B. Bhikkaji, M. Ratnam, and S. O. R. Moheimani, "PVPF control of piezoelectric tube scanners," *Sens. Actuators Phys.*, vol. 135, no. 2, pp. 700-712, Apr. 2007.
- 31  
32 [21] L. Li, C.-X. Li, G. Gu, and L.-M. Zhu, "Positive acceleration, velocity and position feedback based damping control approach for piezo-actuated nanopositioning stages," *Mechatronics*, vol. 47, pp. 97-104, Nov. 2017.
- 33  
34 [22] M. Namavar, A. J. Fleming, M. Aleyaasin, et al., "An Analytical Approach to Integral Resonant Control of Second-Order Systems," *IEEE/ASME Trans. Mechatron.*, vol. 19, no. 2, pp. 651-659, Apr. 2014.
- 35  
36 [23] M.-J. Yang, J.-B. Niu, C.-X. Li, et al., "High-Bandwidth Control of Nanopositioning Stages via an Inner-Loop Delayed Position Feedback," *IEEE Trans. Autom. Sci. Eng.*, vol. 12, no. 4, pp. 1357-1368, Oct. 2015.
- 37  
38 [24] G. M. Clayton, S. Tien, K. K. Leang, Q. Zou, and S. Devasia, "A Review of Feedforward Control Approaches in Nanopositioning for High-Speed SPM," *J. Dyn. Syst. Meas. Control*, vol. 131, no. 6, p. 061101, 2009.
- 39  
40 [25] Y. K. Yong, S. O. R. Moheimani, B. J. Kenton, and K. K. Leang, "Invited Review Article: High-speed flexure-guided nanopositioning: Mechanical design and control issues," *Rev. Sci. Instrum.*, vol. 83, no. 12, p. 121101, Dec. 2012.
- 41  
42 [26] Y. Shan and K. K. Leang, "Accounting for hysteresis in repetitive control design: Nanopositioning example," *Automatica*, vol. 48, no. 8, pp. 1751-1758, Aug. 2012.
- 43  
44 [27] L. Li, Z. Chen, S. S. Aphale, and L. Zhu, "Fractional Repetitive Control of Nanopositioning Stages for High-Speed Scanning Using Low-Pass FIR Variable Fractional Delay Filter," *IEEE/ASME Trans. Mechatron.*, vol. 25, no. 2, pp. 547-557, Apr. 2020.
- 45  
46 [28] Z. Feng, M. Ming, J. Ling, et al., "Fractional delay filter based repetitive control for precision tracking: Design and application to a piezo-
- 47  
48  
49  
50  
51  
52  
53  
54  
55  
56  
57  
58  
59  
60  
61  
62  
63  
64  
65

- 1  
2  
3 electric nan positioning stage, ” *Mech. Syst. Signal Process.*, vol. 164, p. 108249, Feb. 2022.
- 4 [29] H. Xie, Y. Wen, X. Shen, H. Zhang, and L. Sun, “High-Speed AFM Imaging of Nanopositioning Stages Using  $H_\infty$  and Iterative Learning
- 5 Control, ” *IEEE Trans. Ind. Electron.*, vol. 67, no. 3, pp. 2430-2439, Mar. 2020.
- 6 [30] Z. Li and J. Shan, “Modeling and Inverse Compensation for Coupled Hysteresis in Piezo-Actuated FabryCPerot Spectrometer, ” *IEEE/ASME*
- 7 *Trans. Mechatron.*, vol. 22, no. 4, pp. 1903-1913, Aug. 2017.
- 8 [31] M. S. Rana, H. R. Pota, and I. R. Petersen, “Nonlinearity Effects Reduction of an AFM Piezoelectric Tube Scanner Using MIMO MPC, ”
- 9 *IEEE/ASME Trans. Mechatron.*, vol. 20, no. 3, pp. 1458-1469, Jun. 2015.
- 10 [32] M. S. Rana, H. R. Pota, and I. R. Petersen, “Spiral Scanning With Improved Control for Faster Imaging of AFM, ” *IEEE Trans. Nanotechnol.*,
- 11 vol. 13, no. 3, pp. 541-550, May 2014.
- 12 [33] Y. K. Yong, K. Liu, and S. O. R. Moheimani, “Reducing Cross-Coupling in a Compliant XY Nanopositioner for Fast and Accurate Raster
- 13 Scanning, ” *IEEE Trans. Control Syst. Technol.*, vol. 18, no. 5, pp. 1172-1179, Sep. 2010.
- 14 [34] H. Habibullah, H. R. Pota, I. R. Petersen, and M. S. Rana, “Creep, Hysteresis, and Cross-Coupling Reduction in the High-Precision Posi-
- 15 tioning of the Piezoelectric Scanner Stage of an Atomic Force Microscope, ” *IEEE Trans. Nanotechnol.*, vol. 12, no. 6, pp. 1125-1134, Nov.
- 16 2013.
- 17 [35] S. I. Moore, Y. K. Yong, M. Omidbeike, and A. J. Fleming, “Serial-kinematic monolithic nanopositioner with in-plane bender actuators, ”
- 18 *Mechatronics*, vol. 75, p. 102541, May 2021.
- 19 [36] S. K. Das, H. R. Pota, and I. R. Petersen, “Damping Controller Design for Nanopositioners: A Mixed Passivity, Negative-Imaginary, and
- 20 Small-Gain Approach, ” *IEEE/ASME Trans. Mechatron.*, vol. 20, no. 1, pp. 416-426, Feb. 2015.
- 21 [37] L. Li, J. Huang, S. S. Aphale, and L. Zhu, “A smoothed raster scanning trajectory based on acceleration-continuous B-spline transition for
- 22 high-speed Atomic Force Microscopy, ” *IEEE/ASME Trans. Mechatron.*, vol. 26, no. 1, pp. 24-32, 2021.
- 23 [38] S. Tien, Qingze Zou, and S. Devasia, “Iterative control of dynamics-coupling-caused errors in piezoscanners during high-speed AFM opera-
- 24 tion, ” *IEEE Trans. Control Syst. Technol.*, vol. 13, no. 6, pp. 921-931, Nov. 2005.
- 25 [39] Y. Tian, K. Cai, D. Zhang, et al., “Development of a XYZ scanner for home-made atomic force microscope based on FPAA control, ” *Mech.*
- 26 *Syst. Signal Process.*, vol. 131, pp. 222-242, Sep. 2019.
- 27 [40] Z. Feng, W. Liang, J. Ling, et al., “Integral terminal sliding-mode-based adaptive integral backstepping control for precision motion of a
- 28 piezoelectric ultrasonic motor, ” *Mech. Syst. Signal Process.*, vol. 144, p. 106856, Oct. 2020.
- 29 [41] A. V. Oppenheim, R. W. Schafer, and J. R. Buck, “Discrete-time signal processing (2nd ed.), ” *Prentice-Hall, Inc.*, 1999.
- 30  
31  
32  
33  
34  
35  
36  
37  
38  
39  
40  
41  
42  
43  
44  
45  
46  
47  
48  
49  
50  
51  
52  
53  
54  
55  
56  
57  
58  
59  
60  
61  
62  
63  
64  
65

**Declaration of interests**

The authors declare that they have no known competing financial interests or personal relationships that could have appeared to influence the work reported in this paper.

The authors declare the following financial interests/personal relationships which may be considered as potential competing interests: